APL Materials

Two-dimensional spin systems in PECVD-grown diamond with tunable density and long coherence for enhanced quantum sensing and simulation 🄵

Lillian B. Hughes ⬡ ; Zhiran Zhang; Chang Jin ⬡ ; Simon A. Meynell; Bingtian Ye; Weijie Wu; Zilin Wang; Emily J. Davis; Thomas E. Mates; Norman Y. Yao; Kunal Mukherjee ⬡ ; Ania C. Bleszynski Jayich ✉ ⬡

Check for updates

🄯 CHORUS

View Online   Export Citation   CrossMark

Two-dimensional spin systems in PECVD-grown diamond with tunable density and long coherence for enhanced quantum sensing and simulation ⓕ

Lillian B. Hughes,[1] ⓘD Zhiran Zhang,[2] Chang Jin,[2] ⓘD Simon A. Meynell,[2] Bingtian Ye,[3] Weijie Wu,[3] Zilin Wang,[3] Emily J. Davis,[3] Thomas E. Mates,[1] Norman Y. Yao,[4] Kunal Mukherjee,[5] ⓘD and Ania C. Bleszynski Jayich[2,a)] ⓘD

AFFILIATIONS

[1] Materials Department, University of California, Santa Barbara, Santa Barbara, California 93106, USA
[2] Department of Physics, University of California, Santa Barbara, Santa Barbara, California 93106, USA
[3] Department of Physics, University of California, Berkeley, Berkeley, California 94720, USA
[4] Department of Physics, Harvard University, Cambridge, Massachusetts 02138, USA
[5] Department of Materials Science and Engineering, Stanford University, Palo Alto, California 94305, USA

[a)] Author to whom correspondence should be addressed: jayicha@ucsb.edu

ABSTRACT

Systems of spins engineered with tunable density and reduced dimensionality enable a number of advancements in quantum sensing and simulation. Defects in diamond, such as nitrogen-vacancy (NV) centers and substitutional nitrogen (P1 centers), are particularly promising solid-state platforms to explore. However, the ability to controllably create coherent, two-dimensional spin systems and characterize their properties, such as density, depth confinement, and coherence, is an outstanding materials challenge. We present a refined approach to engineer dense ($\gtrsim 1$ ppm · nm), 2D nitrogen, and NV layers in diamond using delta-doping during plasma-enhanced chemical vapor deposition epitaxial growth. We employ both traditional materials techniques, e.g., secondary ion mass spectrometry, alongside NV spin decoherence-based measurements to characterize the density and dimensionality of the P1 and NV layers. We find P1 densities of 5–10 ppm · nm, NV densities between 1 and 3.5 ppm · nm tuned via electron irradiation dosage, and depth confinement of the spin layer down to 1.6 nm. We also observe high (up to 0.74) ratios of NV to P1 centers and reproducibly long NV coherence times, dominated by dipolar interactions with the engineered P1 and NV spin baths.

Solid-state spins constitute a powerful platform for quantum technologies. They can exhibit long quantum coherence, even up to room temperature, are naturally trapped, making them robust and easy to use, and can be simply integrated with sensing targets at nanoscale distances, making them advantageous for quantum sensing.[1–4] Furthermore, dense ensembles of coherent spins provide a starting point for investigating strongly interacting spin systems[5–10] in which novel, many-body states can arise with applications in both quantum simulation and sensing.

Two dimensional confinement of dense, coherent spin ensembles opens up a number of experimental avenues. Dimensionality plays a critical role in the nature of many-body states, with reduced dimensionality giving access to unique phases and phenomena such as interaction-driven localization.[7,11–14] Furthermore, because the 3D angular average of the dipole–dipole interaction yields zero, reduced dimensionality is necessary for collective phenomena such as dipolar-driven spin squeezing[15] and plays an important role in the decoherence dynamics of many-body systems.[16]

For sensing applications, a dense 2D layer of sensors in close proximity to a sensing target exhibits enhanced spatial resolution (set by the depth of the layer) compared to a 3D ensemble at the same volumetric density, while benefiting from either $1/\sqrt{N}$ classical sensitivity enhancements or entanglement-driven enhancements. Finally, dense 2D ensembles could serve as a starting point for the targeted, on demand formation of individual, optically resolvable defects at specific locations, such as inside nanostructures. Altogether, creating thin spin layers with tunable density is of intense current interest but has been minimally explored in solid-state electronic spin systems to date.

In this paper, we explore defects in diamond, an ideal host for solid-state spin qubits. Diamond's wide bandgap of 5.4 eV, high Debye temperature of 2250 K, and predominantly nuclear spin-free ^{12}C composition (when grown synthetically using isotopic engineering) provide an exceptionally quiet lattice environment for a myriad of embedded defects with long quantum coherence. The most well-explored qubit system in diamond is the negatively charged nitrogen-vacancy (NV) defect, whose spin can be easily manipulated and read out at room temperature using optical and microwave radiation and has been leveraged for a number of notable experiments in quantum sensing.[1,2,4] Substitutional nitrogen, known as the P1 center, is another diamond defect that may be used for quantum simulation[16] or building multi-qubit quantum registers[17] when used in conjunction with the optically addressable NV center. While much of the diamond qubit literature focuses on single NV spins for high spatial resolution quantum sensing, and dense ensembles of defects (either NV or P1) are becoming increasingly important for a number of experiments leveraging interacting many-body systems.[16,18] The engineering and characterization of such systems will be the focus of this work.

The creation of tunably dense, coherent, two-dimensional spin layers in diamond is challenging. Ion implantation, the most commonly used method for forming depth-confined defects, suffers from two challenges. First, the high energy of the implanted ions results in decoherence-producing collateral damage (e.g., vacancy-related defects),[19] which is exacerbated by the large implantation dosages necessary to achieve high spin densities. Second, implantation results in a broadened depth distribution of the implanted element. Thin layer confinement can be improved with lower energy implantation, but the spread of depths of these shallowly implanted defects has been observed to be greater than that predicted by SRIM simulations.[20,21] More fundamentally, defect properties degrade significantly near the surface,[22] which is particularly undesirable for quantum simulation, where spin–spin interactions must dominate over external decoherence sources. Overgrowth after shallow implantation is a path toward improved coherence but risks passivation and loss of defects during the growth.[23]

An alternative pathway toward engineering dense, thin spin layers is delta-doping during plasma-enhanced chemical vapor deposition (PECVD) diamond growth. This technique, pioneered by Ohno et al.[24] for low density ($\lesssim 0.1$ ppm · nm) layers and further employed by others,[25–29] allows for control over the dopant thickness and density in a gentle, bottom-up approach that can preserve long coherence. Vacancy-related defects can be subsequently promoted via a variety of irradiation methods for further tunability of defect density and location. To date, the growth and irradiation approach has predominantly focused on the creation of 3D ensembles,[30,31] with only a few studies investigating dense ($\gtrsim 1$ ppm · nm), thin defect layers where spin–spin interactions may become relevant.[16,25,32]

In this work, we create highly confined two-dimensional nitrogen layers in diamond via delta-doping during PECVD growth. Benefiting from an increased understanding of nitrogen incorporation, we identify a set of growth parameters that yields depth confinement of the doped nitrogen layer down to 1.6 nm, as measured by secondary ion mass spectrometry (SIMS). We further confirm the 2D nature of the nitrogen spins via spin-based sensing methods, specifically via the decoherence profile of colocalized NV center probe qubits, which are formed via 200 keV electron irradiation and annealing. We next use several methods to quantify the P1 and NV densities and discuss their relative merits. From the timescale of the NV qubit decoherence, we measure the P1 density to be 5–10 ppm · nm. This density measurement is notably 6–8 times smaller than the nitrogen density extracted by SIMS, and we put forth reasoning in support of the accuracy of the qubit-based measurements. To estimate the NV density, we introduce a new, simple Rabi contrast-based method and benchmark it against other qubit-based density estimation techniques. With the Rabi-assisted fluorescence method, we measure an NV density of 1–3.5 ppm · nm, tuned via electron irradiation dosage. We find a high NV/P1 ratio of up to 0.74 and propose a model to support the increased conversion for a 2D nitrogen layer. Importantly, the NV centers show reproducibly long coherence times, both for ensembles and single NVs, and we find that the coherence is predominantly limited by spin–spin interactions within the dense P1 and NV bath. Altogether, this work presents a joint materials and qubit-based approach to engineer and characterize interesting spin systems for applications in quantum technologies.

## I. MATERIAL GROWTH, CHARACTERIZATION, AND PREPARATION

A. PECVD diamond growth and nitrogen delta-doping

Creating nanometer-scale layers and interfaces via *in situ* doping during PECVD diamond growth is typically difficult with fast growth rates, on the order of a few μm/h, and the residual time of the dopant gas.[33] Here we adopt a slow growth approach that allows for precise depth control and promotes high epitaxial quality of the diamond film. Through the use of a low power (750 W, 25 Torr) plasma, a low methane concentration (0.1% of the 400 sccm H_2 flow), and a sample holder temperature of ~750 °C as measured via a pyrometer, we achieve a slow epitaxial growth rate of 10–30 nm/h. The diamond epilayers are grown on (100) oriented electronic grade diamond substrates (Element Six Ltd.). Prior to growth, substrates are fine-polished by Syntek Ltd. to a surface roughness of ~200–300 pm and also undergo a 4–5 μm etch to relieve polishing-induced strain.

During the nitrogen delta-doping period of growth, all plasma conditions are held constant, and $^{15}N_2$ gas (1.25% of the total gas content) is introduced into the chamber briefly to create a delta-doped layer. Optical emission spectroscopy (OES) is used to record the residual time of nitrogen in the chamber following doping, which is found to be just 22 s. The $^{15}N_2$ doping time in this work is set to 15 min; however, the delta-layer thickness is less than expected given

the pre-doping growth rate. This observation contrasts the assertion that nitrogen doping enhances growth rates[34] and suggests that during the delta-doping phase, the plasma chemistry changes significantly such that steady growth is slowed or interrupted. Further investigation is needed to better understand the growth rate discontinuity that allows for thin layer creation and will be the subject of future work. The ^{15}N isotope is used to spectroscopically distinguish doped P1 and NV centers from the 99.6% natural abundance ^{14}N isotope in the substrate via differences in hyperfine coupling to the N nuclear spin. We use isotopically purified methane (99.999% $^{12}CH_4$, Cambridge Isotope Laboratories) to engineer a diamond lattice environment composed of 99.998% ^{12}C, as measured by SIMS [Fig. 1(a)], thus largely removing ^{13}C, an isotope with nonzero nuclear spin that contributes magnetic noise and induces NV center decoherence.

A number of parameters are known to affect the density of nitrogen incorporated during growth, including the growth temperature,[35] the gas flow ratios,[28] and the misorientation angle of the seed substrate.[28,36] We find that the epitaxial growth rate, which
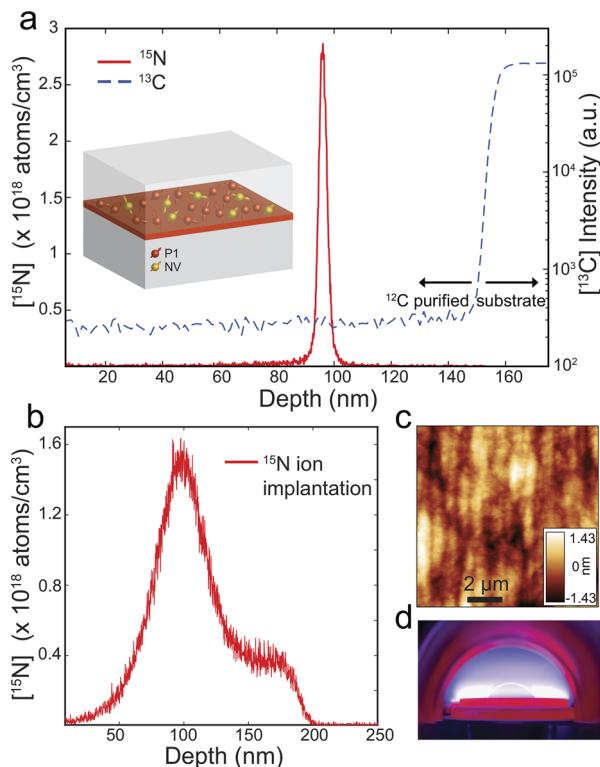
FIG. 1. (a) SIMS depth profile of PECVD-grown diamond sample A, showing the ^{15}N (collected as a $^{12}C^{15}N^-$ ion) and ^{13}C composition as a function of depth. The FWHM of the dopant layer is 3.55(0.04) nm, and the areal density of the peak = 1.057(0.009) × 10^{12} atoms/cm^2 or 60.1(0.5) ppm · nm when integrated over a range of ±3σ. Inset shows a schematic of a two-dimensional spin system consisting of P1 and NV centers in a delta-doped layer. (b) SIMS depth profile of a ^{15}N ion implanted sample (90 keV, 1 × 10^{13} e$^-$/cm^2 dose), showing significant broadening compared to the delta-doped sample shown in (a). (c) AFM image of grown sample A, illustrating surface roughness S_q < 0.5 nm over a 100 μm^2 region. (d) Image of the PECVD plasma during diamond growth.

encompasses the effect of all of these parameters, displays the most clear relationship to nitrogen incorporation. To control the growth rate, and hence nitrogen incorporation, we modify the miscut angle of the substrate following recent work[36] while keeping temperature and gas flow rates constant. We specify the miscut angle by first measuring the virgin substrates using x-ray diffractometry (XRD) rocking curve measurements about the (004) omega peak and subsequently using off-angle fine polishing (Syntek Ltd.) to target a 1.0°–1.5° miscut. In this miscut range, we observe increased nitrogen incorporation with an increased growth rate.

After growth, the diamonds are further electron irradiated and annealed to generate enhanced NV center concentrations. Irradiation is performed with the 200 keV electrons of a transmission electron microscope (TEM, ThermoFisher Talos F200X G2 TEM). This energy is just above the carbon atom displacement threshold energy of 145 keV for (100) diamond,[29,37] thus allowing us to target the formation of single vacancies and minimize extended lattice damage that may occur with higher energies.[38] The irradiation time is varied to create spots that range in dose from 10^{18}–10^{21} e$^-$/cm^2. The samples then undergo subsequent annealing at 850 °C for 6 h in an Ar/H$_2$ atmosphere, during which the vacancies diffuse and form NV centers. After irradiation and annealing, the samples are cleaned in a boiling piranha solution (3:1 H$_2$SO$_4$:H$_2$O$_2$) to remove surface contaminants and help stabilize the negative NV$^-$ charge state for further measurements. All data in the main text of this paper were taken on one sample (sample A). To demonstrate the repeatability of our growth, preparation, and characterization techniques, we present data on a second, similarly prepared sample (sample B) in the supplementary material.

B. Secondary ion mass spectrometry analysis

The primary bulk materials characterization tool for depth-resolved elemental analysis is SIMS, in which a primary ion beam is directed at a sample, sputtering away material and collecting information about the elemental and isotopic composition as a function of depth. We use a CAMECA IMS 7f dynamic SIMS instrument with a primary Cs$^+$ beam energy of 7 kV and a current of ~30 nA at an incident angle of 21.7° to achieve a sputtering rate of ~20 nm/min. The sample is biased to −3000 V, and $^{12}C^{15}N^-$ negative secondary ions are detected using a high mass resolving power, M/ΔM = 6006. Only ions from the central 33 μm are collected from the 100 μm sputtering crater to avoid edge effects. We observe a delta-doped layer of thickness 3.55(0.04) nm, as determined from the full width at half-maximum (FWHM) of the peak in the nitrogen depth profile illustrated in Fig. 1(a). The error represents a 95% confidence interval for a Gaussian peak fit. Importantly, the thickness of this layer is significantly narrower than that of a sample in which nitrogen was introduced via a standard implantation technique targeting a similar depth, as can be seen in Fig. 1(b). This sample was implanted with ^{15}N ions at 90 keV, 1 × 10^{13} dose e$^-$/cm^2, and a 7° tilt to mitigate ion channeling. However, channeling is still observed in the SIMS data, as evidenced by the peak's shoulder extending out to 200 nm depth. The FWHM of the main peak at 100 nm depth fit with a Gaussian is 53.3(0.2) nm, which is significantly broader than the delta-doped layer, and furthermore broadened compared to the expected 42.2 nm FWHM predicted by SRIM simulation.[39]

SIMS depth resolution is limited by the sample's surface roughness, which causes ion mixing at the doped layer interface, and

thus the 3.5 nm thickness of sample A is convolved with its surface roughness [Fig. 1(c)] and may represent an upper bound. However, under similar SIMS measurement parameters, we have observed an even thinner layer of 1.61(0.02) nm thickness in a different sample grown with a shorter, five-minute doping time [supplementary material Fig. S1(a)]. This observation suggests that the SIMS resolution may not be the dominant limitation in our measurement, but without a secondary characterization, the exact layer thickness remains unknown.

From the SIMS data, we can also extract a quantitative estimate of the dopant density by comparing the signal strength to a reference standard with a known dopant dose introduced by ion implantation and calculating a relative sensitivity factor (RSF). Taking the background ^{12}C matrix into account and assuming similar instrumental conditions between runs, the RSF can be used to determine the atomic concentrations of the doped nitrogen. Further details on the RSF calibration are given in the supplementary material. We integrate over three standard deviations of a Gaussian-fit peak shown in Fig. 1(a) to calculate an areal density of $1.057(0.009) \times 10^{12}$ atoms/cm^2 or 60.1(0.5) ppm · nm. Notably, this density should be considered as an estimate only due to the run-to-run variability in beam tuning, sample charging/surface potentials, and mounting conditions, which may cause non-uniform fields.[40] Additionally, SIMS measures all nitrogen and does not discriminate between different N-related defects, so the extracted density likely overestimates the exact substitutional nitrogen (P1 center) content.

While SIMS is an important tool for the characterization of delta layers, the shortcomings in estimating doping thickness and concentration require cross-reference with another measurement. However, the sensitivities of conventional techniques such as transmission electron microscopy (TEM), energy-dispersive x-ray spectroscopy (EDS), or even standard bulk electron paramagnetic resonance (EPR) are generally not low enough to detect the nitrogen densities of delta layers in diamond. We note that recent developments in superconducting microcavity based EPR do achieve the required sensitivities[41] but are still very challenging to implement. Furthermore, the insulating nature and hardness of diamond often make ion beam techniques difficult.[26] These challenges point toward the need for an alternate characterization route that achieves greater sensitivity in a non-destructive manner, thus leading us to use the NV center itself as a probe of its surrounding lattice.

II. CHARACTERIZATION OF THE SUBSTITUTIONAL NITROGEN SPIN BATH

NV centers serve as excellent sensors of the local spin environment via dipolar interactions with nearby spins. In this work, we use the decoherence dynamics of a probe NV center ensemble to reveal characteristics of the surrounding P1 bath. We utilize double electron–electron resonance (DEER) and Hahn spin echo measurements to accurately quantify the P1 center density, ρ_{P1},[16,30,42] and confirm their dimensionality.[16] Two-dimensionality is defined by a layer thickness that is smaller than the inter-spin spacing for a given dopant density. Figure 2(a) shows a photoluminescence image of the TEM-irradiated, NV-rich spot on sample A (henceforth referred to as spot I). All NV-based measurements are performed on a home-built confocal microscope using a 532-nm diode laser and an external magnetic field of ~320 G aligned along one of the

NV ⟨111⟩ axes. Radio frequency (RF) signals are delivered through a gold antenna fabricated on a glass cover slip and placed underneath the diamond.

A. Extraction of density and dimensionality

Through DEER-based sensing, we characterize the nitrogen spin bath by selectively probing the quasistatic contribution of P1 centers to NV decoherence. Figure 2(b) shows a frequency-swept DEER spectrum of the $m_I = -\frac{1}{2}$ hyperfine state of the ^{15}N P1 centers[30] revealing two peaks: the shallow peak (the 1/8 group) corresponds to the ^{15}N P1 center with its Jahn–Teller axis aligned to the external magnetic field and the deeper peak (the 3/8 group) corresponds to the three other degenerate ^{15}N P1 centers with Jahn–Teller axes misaligned to the field.[43] The DEER pulse sequence is illustrated in the inset of Fig. 2(b). A pump pulse resonant with the 3/8 group of P1 centers with frequency f_{P1} recouples the P1 bath to the NV centers, and the resulting contribution to decoherence is read out via an NV center Hahn echo measurement. Essentially, this sequence constitutes a Ramsey measurement of the NV–P1 interaction.

The timescale of the DEER decoherence decay provides information about the density of P1 centers, and the stretch exponent of the decay indicates the dimensionality of the spin bath. According to the theory presented in Ref. 16, the decoherence decay profile is expected to take the following form:

$$C(t) \approx \exp[-\rho_{3/8}[aJ(2\tau)]^n], \qquad (1)$$

where $\rho_{3/8}$ is the density (in units of ppm · nm for a 2D spin bath) of the driven group of P1 centers, a is a dimensionless constant (that equals 2.626 for a 2D spin bath or 3.318 for a 3D spin bath), and $J = 2\pi \times 52$ MHz nm^3 is the dipolar coupling strength. The stretch power, $n = d/\alpha$, depends on the dimensionality of the system, d, and the power law of the interactions, α. Importantly, Eq. (1) is only valid at times short compared to the correlation time τ_c of the bath, i.e., $\tau \ll \tau_c$. For a 2D spin bath coupled to the NV via dipolar interactions ($\alpha = 3$), we expect $n = 2/3$ when measuring on a time scale much shorter than τ_c; for a 3D bath, we expect $n = 1$ as seen, e.g., in Ref. 16. Further details on the theoretical analysis are given in the supplementary material.

Figure 2(c) plots the NV coherence as measured by Hahn echo and by DEER using a differential measurement scheme.[44] The DEER data show the expected reduction in coherence when recoupling the P1 centers. Figure 2(d) plots the DEER decay normalized by the NV Hahn echo on a log–log scale as a function of free evolution time (2τ). The DEER data are normalized by the Hahn echo in order to eliminate any contributions to decoherence from other sources. The excellent agreement of the data to a fit with a stretch power of $n = 2/3$ and poor agreement with $n = 1$ confirms the two-dimensional nature of the spins.

The data also provide a quantitative estimate of the total P1 density, $\rho_{P1} = 7.6 \pm 1.8$ ppm · nm in TEM irradiation spot I. This density corresponds to a P1 spacing of ~13.8 nm, larger than the layer thickness as measured by SIMS and hence consistent with a 2D spin system. Density measurements are averaged over six locations within TEM spot I, where the 1.8 ppm · nm standard deviation reflects the ρ_{P1} variation across the spot. We attribute this variation
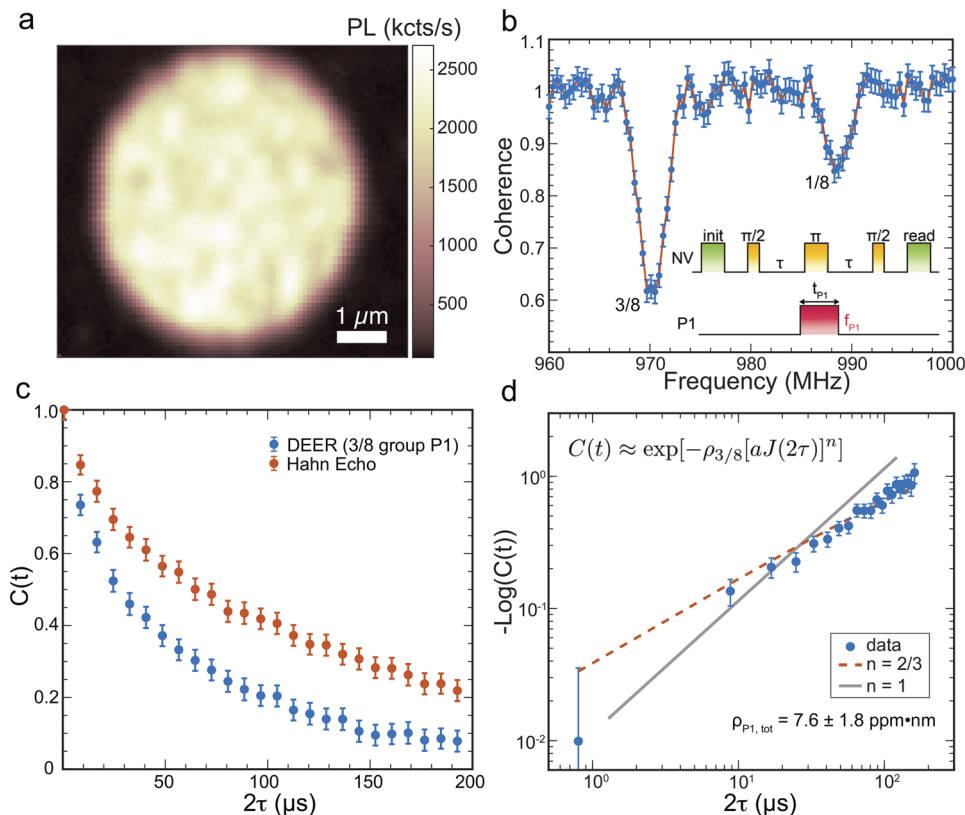
FIG. 2. (a) Photoluminescence image of a 5-μm diameter TEM-irradiated spot (5.4×10^{19} e$^-$/cm^2 dose) on sample A, taken with an excitation power of ~1.3 mW (half saturation) measured at the confocal back aperture. This spot is further referred to as spot I in the text. (b) Frequency-swept DEER spectrum of P1 centers at B = 322 G aligned along one of the $\langle 111 \rangle$ directions. The frequency range is chosen to zoom in on the ^{15}N $m_I = -1/2$ hyperfine manifold. Inset shows the pulse sequence. The duration of the P1 pulse t_{P1} is set to 300 ns while its frequency f_{P1} is swept. The deep (shallow) peak corresponds to the 3/8 (1/8) group of P1 centers. The orange line shows a fit to the data. (c) Hahn echo coherence decay of the probe NV centers as a function of total free evolution time 2τ with (blue) and without (orange) recoupling of the 3/8 P1 group. Error bars represent the standard error of the mean. (d) Log–log plot of the DEER coherence decay normalized by the Hahn echo data. The orange dashed line shows the best fit for a stretch exponent of $n = 2/3$, expected for a 2D bath. For comparison, the best fit for $n = 1$ (a 3D spin bath) is also plotted. The 2D fit with Eq. (1) yields a total P1 areal density $\rho_{P1} = 7.6 \pm 1.8$ ppm · nm.

to inhomogeneous nitrogen incorporation during growth, which will be the subject of future study. We note that the NV-DEER based estimate of ρ_{P1} is ~8 times lower than the SIMS measurement [60.1(0.5) ppm · nm]. This trend holds for the data collected on sample B as well, where the DEER-measured ρ_{P1} of 16 ppm · nm is ~6 times less than the SIMS-estimated 89.5(0.8) ppm · nm (full analysis in the supplementary material). Given the uncertainties in the RSF value and the fact that SIMS measures all forms of nitrogen and is not specifically sensitive to P1 centers (as in DEER), this discrepancy is not surprising, and importantly, it confirms our understanding that SIMS needs a cross-referencing technique to more accurately determine the concentration of dopant atoms in our material.

III. CHARACTERIZATION OF NV CENTER PROPERTIES

We next move to characterizing the density, dimensionality, and coherence of NV centers formed via our growth and irradiation approach. In addition to enabling the study of strongly interacting, optically addressable spin ensembles in 2D for sensing and simulation, it also facilitates the creation of coherent NV centers with a specified, tunable density to realize, e.g., a single NV per nanopillar in a scanning probe tip[45,46] or a single NV inside of a photonic crystal cavity.[47] Here we explore the creation and properties of the NV centers in our delta-doped system, finding both high NV/P1 ratios and remarkably long coherence, which is predominantly limited by the P1 and NV environment.

A. NV center density estimation

A number of methods are typically used to estimate the NV center density, ρ_{NV}, when individual NV centers are not optically resolvable and countable. Broadly, these methods fall into two categories: the first involves probing the decoherence timescale of the NV ensemble under a specific RF pulse sequence, such as NV–NV DEER,[30] instantaneous diffusion,[30] or an XY-8 sequence.[18] The second, all-optical method estimates density from the ensemble fluorescence intensity. However, these techniques all come with their drawbacks. The spin decoherence methods require long averaging times and are limited to dense NV ensembles where NV–NV dipolar interactions are comparable to or stronger than other sources of decoherence. Biased estimates can result when ensembles deviate from this high (NV-dominant) density, and pulse errors can introduce further bias (see the supplementary material for a further explanation and the results of implementing these methods on samples A and B). Estimating the density of NV ensembles via fluorescence can be hampered by unwanted background fluorescence from other irradiation-induced defects, which becomes particularly relevant at high electron dosages.

Here we introduce a simple and more reliable approach to determine the NV density. Our method benefits from not only its quick and easy implementation but also its large dynamic range, which allows for density estimation from single NVs to high-density ensembles. We measure the fluorescence intensity difference between NV ensemble spin states ($m_s = 0$ and $m_s = \pm 1$) in a Rabi

experiment and normalize by the corresponding signal from a single NV. By isolating the component of the fluorescence that changes with microwave driving, the measurement is immune to contributions from non-NV$^-$ defects. This method combines fluorescence counting and spin manipulation to measure a uniquely NV signal.

Briefly, our NV density estimation technique proceeds as follows (further details are provided in the supplementary material). First, the point spread function (PSF) of the confocal setup is determined by fitting the fluorescence profile of an average of several single NV centers. Next, the PSF is convolved with a random distribution of 1 ppm · nm NVs to calculate a spatial average of the resulting signal, f_{avg}. This average factor accounts for the fact that not all NV centers in the confocal spot reside at the center of the spot. Finally, ρ_{NV} is estimated by relating ΔPL_R, the fluorescence intensity difference of the $m_s = 0$ and ± 1 states in a Rabi experiment, of single and ensemble NVs via,

$$\rho_{NV} = \frac{\Delta PL_{R,NVensemble}}{\Delta PL_{R,singleNV}} \times \frac{1}{f_{avg}} \times 4. \qquad (2)$$

The factor of four accounts for the four possible NV orientations, assuming an equal distribution among them, to yield ρ_{NV} as the total NV density.

Applying this method to the TEM spot I, we find $\rho_{NV} = 2.6 \pm 0.9$ ppm · nm averaged over eight different laser positions within the spot. The variation of ρ_{NV} across the spot is consistent with the variation observed in ρ_{P1}. In the supplementary material, we compare measurements of ρ_{NV} in samples A and B obtained with our Rabi-assisted fluorescence method and spin decoherence methods, specifically NV–NV DEER and XY-8. Using our new method, we find ρ_{NV} to lie between the estimates produced by NV–NV DEER and XY-8 measurements; this trend is consistent with our expectations for the biases imposed by these two methods and advocates for the accuracy of our Rabi-assisted fluorescence measurement.

B. NV center creation and coherence

We next characterize ρ_{NV} across a range of electron irradiation dosages and, importantly, find a high NV/P1 ratio of up to 0.74, corresponding to ρ_{NV} of up to 3.5 ± 0.4 ppm · nm. Figures 3(a) and 3(b) show a clear increasing trend of ρ_{NV} and NV/P1 ratio with electron dosage. The NV/P1 ratio is an important figure of merit for this work because the NV and P1 centers are the dominant contributors to decoherence in our samples, as will be discussed below. Furthermore, ρ_{NV} and ρ_{P1} are quantitatively probed by our NV-based measurements. Interestingly, we observe higher NV/P1 ratios in our 2D delta-doped sample compared to 3D nitrogen-doped samples prepared via similar irradiation dosages and growth procedures (with longer doping times).[30] We posit that the higher NV/P1 ratios observed here are related to the dimensionality of the nitrogen layer and the diffusion of vacancies during annealing. In a 2D layer, each nitrogen interacts with a greater number of vacancies compared to the 3D case because of the finite diffusion volume during annealing. Thus, the enhancement will be determined by a dimensionless parameter given by V_D/t_L, where V_D is the diffusion volume and t_L is the layer thickness.

To test the validity of this explanation, we construct a simple vacancy capture model (detailed in the supplementary material) where vacancies migrate according to a weighted one-dimensional
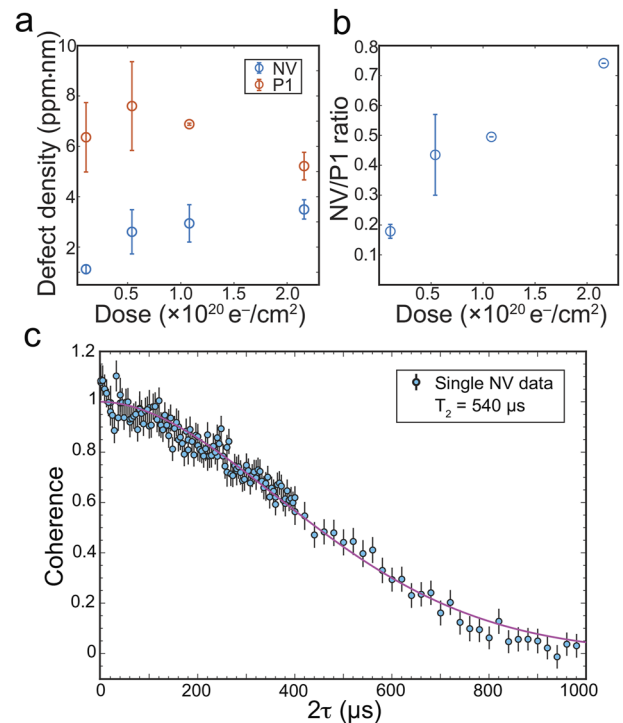
FIG. 3. (a) Plot of the ρ_{P1} and ρ_{NV} (measured with DEER and Rabi-assisted fluorescence counting, respectively) as a function of electron irradiation dose. Error bars show the standard error of the mean. (b) NV/P1 ratio as a function of electron irradiation dose. Small standard error bars are due to a small sample size. (c) Hahn echo decay for a single NV center outside of the TEM spots illustrating a T_2 of 540 μs.

random walk and can be captured by adjacent nitrogen with unit probability. Using our experimental parameters, we find a 15× enhancement of conversion for the 2D layer vs the 3D layer, supporting the hypothesis that the geometrical diffusion effect is responsible for the observed enhancement in 2D. While this model does not attempt to rigorously simulate all aspects of the NV center formation process, it supports our experimental findings of increased conversion in 2D-doped samples and suggests an interesting subject for future study.

Beyond the high NV/P1 ratios, a notable feature of the NV centers in our delta-doped samples is their long Hahn echo T_2 coherence time across a range of P1 and NV defect densities (see supplementary material Fig. S5). Maintaining long coherence is crucial for all the aforementioned experiments and applications in quantum sensing and simulation, particularly when operating in the dense P1 or NV regime. In the unirradiated regions, we find single, optically resolvable delta-doped NV centers in a dense P1 background, and we measure Hahn echo T_2 times of 535, 562, and 489 μs for three single NVs, a representative example of which is shown in Fig. 3(c). This result is promising for applications such as NV scanning probe microscopy, which demands single-NV-containing probes formed with high yield. Higher density ensembles of NV centers in TEM spot I show an average coherence time of 108 ± 10 μs, which is in good agreement with the expected decoherence from

15 March 2024 18:23:23

a bath of P1 and NV centers of the measured density (see the supplementary material for analysis of the P1 and NV contributions to decoherence). The dominance of intentional spin–spin interactions, combined with the system's 2D nature, is critical for experiments in many-body sensing and simulation.

IV. CONCLUSION

In this work, we have demonstrated the controlled creation and characterization of 2D spin systems in diamond with tunable density and long coherence. By harnessing slow growth rates and substrate miscut control, we achieve thin nitrogen layer confinement and characterize the P1 dimensionality and density with both SIMS and NV spin decoherence-based techniques, noting the importance of spin-based measurements in characterizing the relevant spin bath density. We demonstrate NV density tunable via electron irradiation and observe high NV/P1 ratios in the 2D system. NV density characterization is performed using a simple Rabi-assisted, fluorescence-based NV method introduced here that does not suffer from the biases of other estimation techniques and demonstrates a large dynamic range. Furthermore, we observe long NV T_2 coherence times despite the rich P1 and NV environment, suggesting that the system is not severely limited by disorder from other defects. Altogether, this work presents a careful materials and qubit-joint approach to engineer unique spin systems for enabling a variety of investigations in quantum sensing and simulation.

SUPPLEMENTARY MATERIAL

See the supplementary material for additional details on the SIMS analysis, characterization of sample B, details of the Rabi-assisted density estimation and comparison to other methods, the vacancy diffusion/NV creation model, additional coherence measurements and interpretation, and supplementary material about the decoherence decay analysis.

AUTHOR DECLARATIONS

Conflict of Interest

The authors have no conflicts to disclose.

Author Contributions

Lillian B. Hughes: Conceptualization (equal); Investigation (equal); Methodology (equal); Writing – original draft (lead); Writing – review & editing (equal). **Zhiran Zhang**: Formal analysis (equal); Investigation (equal); Methodology (equal); Writing – review & editing (equal). **Chang Jin**: Investigation (equal). **Simon A. Meynell**: Methodology (equal); Writing – review & editing (equal). **Bingtian Ye**: Formal analysis (equal). **Weijie Wu**: Investigation (equal). **Zilin Wang**: Investigation (equal). **Emily J. Davis**: Formal analysis (equal). **Thomas E. Mates**: Methodology (equal). **Norman Y. Yao**: Conceptualization (equal); Funding acquisition (equal); Supervision (equal). **Kunal Mukherjee**: Conceptualization (equal); Funding acquisition (equal); Supervision (equal); Writing – review & editing (equal). **Ania C. Bleszynski Jayich**: Conceptualization (equal); Funding acquisition (equal); Methodology (equal); Supervision (equal); Writing – review & editing (equal).

DATA AVAILABILITY

The data that support the findings of this study are available from the corresponding author upon reasonable request.

REFERENCES

[1] C. L. Degen, F. Reinhard, and P. Cappellaro, "Quantum sensing," Rev. Mod. Phys. **89**, 035002 (2017).

[2] R. Schirhagl, K. Chang, M. Loretz, and C. L. Degen, "Nitrogen-vacancy centers in diamond: Nanoscale sensors for physics and biology," Annu. Rev. Phys. Chem. **65**, 83–105 (2014).

[3] L. Rondin, J.-P. Tetienne, T. Hingant, J.-F. Roch, P. Maletinsky, and V. Jacques, "Magnetometry with nitrogen-vacancy defects in diamond," Rep. Prog. Phys. **77**, 056503 (2014).

[4] F. Casola, T. V. D. Sar, and A. Yacoby, "Probing condensed matter physics with magnetometry based on nitrogen-vacancy centres in diamond," Nat. Rev. Mater. **3**, 17088 (2018).

[5] J. Rovny, R. L. Blum, and S. E. Barrett, "Observation of discrete-time-crystal signatures in an ordered dipolar many-body system," Phys. Rev. Lett. **120**, 180603 (2018).

[6] P. Cappellaro and M. D. Lukin, "Quantum correlation in disordered spin systems: Applications to magnetic sensing," Phys. Rev. A **80**, 032311 (2009).

[7] N. Y. Yao, C. R. Laumann, S. Gopalakrishnan, M. Knap, M. Müller, E. A. Demler, and M. D. Lukin, "Many-body localization in dipolar systems," Phys. Rev. Lett. **113**, 243002 (2014).

[8] S. Choi, J. Choi, R. Landig, G. Kucsko, H. Zhou, J. Isoya, F. Jelezko, S. Onoda, H. Sumiya, V. Khemani, C. von Keyserlingk, N. Y. Yao, E. Demler, and M. D. Lukin, "Observation of discrete time-crystalline order in a disordered dipolar many-body system," Nature **543**, 221–225 (2017).

[9] J. Choi, H. Zhou, H. S. Knowles, R. Landig, S. Choi, and M. D. Lukin, "Robust dynamic Hamiltonian engineering of many-body spin systems," Phys. Rev. X **10**, 031002 (2020).

[10] K. M. Salikhov, S. A. Dzuba, and A. M. Raitsimring, "The theory of electron spin-echo signal decay resulting from dipole–dipole interactions between paramagnetic centers in solids," J. Magn. Reson. **42**, 255–276 (1981).

[11] N. Y. Yao, M. P. Zaletel, D. M. Stamper-Kurn, and A. Vishwanath, "A quantum dipolar spin liquid," Nat. Phys. **14**, 405–410 (2018).

[12] L. Chomaz, D. Petter, P. Ilzhöfer, G. Natale, A. Trautmann, C. Politi, G. Durastante, R. M. W. van Bijnen, A. Patscheider, M. Sohmen, M. J. Mark, and F. Ferlaino, "Long-lived and transient supersolid behaviors in dipolar quantum gases," Phys. Rev. X **9**, 021012 (2019).

[13] A. L. Burin, "Many-body delocalization in strongly disordered system with long-range interactions: Finite size scaling," Phys Rev B **91**, 094202 (2015).

15 March 2024 18:23:23

[14]D. A. Abanin, E. Altman, I. Bloch, and M. Serbyn, "Colloquium: Many-body localization, thermalization, and entanglement," Rev. Mod. Phys. **91**, 021001 (2019).

[15]M. A. Perlin, C. Qu, and A. M. Rey, "Spin squeezing with short-range spin-exchange interactions," Phys. Rev. Lett. **125**, 223401 (2020).

[16]E. Davis, B. Ye, F. Machado, S. Meynell, T. Mittiga, W. Schenken, M. Joos, B. Kobrin, Y. Lyu, D. Bluvstein, S. Choi, C. Zu, A. C. Bleszynski Jayich, and N. Y. Yao, "Probing many-body noise in a strongly interacting two-dimensional dipolar spin system," arxiv:2103.12742 (2021).

[17]M. J. Degen, S. J. H. Loenen, H. P. Bartling, C. E. Bradley, A. L. Meinsma, M. Markham, D. J. Twitchen, and T. H. Taminiau, "Entanglement of dark electron-nuclear spin defects in diamond," Nat. Commun. **12**, 3470 (2021).

[18]H. Zhou, J. Choi, S. Choi, R. Landig, A. M. Douglas, J. Isoya, F. Jelezko, S. Onoda, H. Sumiya, P. Cappellaro, H. S. Knowles, H. Park, and M. D. Lukin, "Quantum metrology with strongly interacting spin systems," Phys. Rev. X **10**, 031003 (2020).

[19]J.-P. P. Tetienne, R. W. D. Gille, D. A. Broadway, T. Teraji, S. E. Lillie, J. M. McCoey, N. Dontschuk, L. T. Hall, A. Stacey, D. A. Simpson, and L. C. L. Hollenberg, "Spin properties of dense near-surface ensembles of nitrogen-vacancy centers in diamond," Phys. Rev. B **97**, 085402 (2018).

[20]S. Kawai, H. Yamano, T. Sonoda, K. Kato, J. J. Buendia, T. Kageura, R. Fukuda, T. Okada, T. Tanii, T. Higuchi, M. Haruyama, K. Yamada, S. Onoda, T. Ohshima, W. Kada, O. Hanaizumi, A. Stacey, T. Teraji, S. Kono, J. Isoya, and H. Kawarada, "Nitrogen-terminated diamond surface for nanoscale NMR by shallow nitrogen-vacancy centers," J. Phys. Chem. C **123**, 3594–3604 (2019).

[21]D. Bluvstein, Z. Zhang, and A. C. Bleszynski Jayich, "Identifying and mitigating charge instabilities in shallow diamond nitrogen-vacancy centers," Phys. Rev. Lett. **122**, 076101 (2019).

[22]B. A. Myers, A. Das, M. C. Dartiailh, K. Ohno, D. D. Awschalom, and A. C. Bleszynski Jayich, "Probing surface noise with depth-calibrated spins in diamond," Phys. Rev. Lett. **113**, 027602 (2014).

[23]C. Findler, J. Lang, C. Osterkamp, M. Nesládek, and F. Jelezko, "Indirect over-growth as a synthesis route for superior diamond nano sensors," Sci. Rep. **10**, 22404 (2020).

[24]K. Ohno, F. Joseph Heremans, L. C. Bassett, B. A. Myers, D. M. Toyli, A. C. Bleszynski Jayich, C. J. Palmstrøm, and D. D. Awschalom, "Engineering shallow spins in diamond with nitrogen delta-doping," Appl. Phys. Lett. **101**, 082413 (2012).

[25]S. Bogdanov, A. Gorbachev, D. Radishev, A. Vikharev, M. Lobaev, S. Bolshed-vorskii, V. Soshenko, S. Gusev, D. Tatarskiy, and A. Akimov, "Investigation of high-density nitrogen vacancy center ensembles created in electron-irradiated and vacuum-annealed delta-doped layers," Phys. Status Solidi RRL **15**, 2000550 (2021).

[26]T. Jaffe, M. Attrash, M. K. Kuntumalla, R. Akhvlediani, S. Michaelson, L. Gal, N. Felgen, M. Fischer, J. P. Reithmaier, C. Popov, A. Hoffman, and M. Orenstein, "Novel ultra localized and dense nitrogen delta-doping in diamond for advanced quantum sensing," Nano Lett. **20**, 3192–3198 (2020).

[27]M. A. Lobaev, A. M. Gorbachev, S. A. Bogdanov, A. L. Vikharev, D. B. Radishev, V. A. Isaev, V. V. Chernov, and M. N. Drozdov, "Influence of CVD diamond growth conditions on nitrogen incorporation," Diamond Relat. Mater. **72**, 1–6 (2017).

[28]M. A. Lobaev, A. M. Gorbachev, S. A. Bogdanov, A. L. Vikharev, D. B. Radishev, V. A. Isaev, and M. N. Drozdov, "NV-center formation in single crystal diamond at different CVD growth conditions," Phys. Status Solidi A **215**, 1800205 (2018).

[29]C. A. McLellan, B. A. Myers, S. Kraemer, K. Ohno, D. D. Awschalom, and A. C. Bleszynski Jayich, "Patterned formation of highly coherent nitrogen-vacancy centers using a focused electron irradiation technique," Nano Lett. **16**, 2450–2454 (2016).

[30]T. R. Eichhorn, C. A. McLellan, and A. C. Bleszynski Jayich, "Optimizing the formation of depth-confined nitrogen vacancy center spin ensembles in diamond for quantum sensing," Phys. Rev. Mater. **3**, 113802 (2019).

[31]D. Farfurnik, N. Alfasi, S. Masis, Y. Kauffmann, E. Farchi, Y. Romach, Y. Hovav, E. Buks, and N. Bar-Gill, "Enhanced concentrations of nitrogen-vacancy centers in diamond through tem irradiation," Appl. Phys. Lett. **111**, 123101 (2017).

[32]S. A. Bogdanov, A. M. Gorbachev, D. B. Radishev, A. L. Vikharev, M. A. Lobaev, S. A. Gusev, D. A. Tatarsky, S. V. Bolshedvorskii, A. V. Akimov, and V. V. Chernov, "Creation of localized NV center ensembles in CVD diamond by electron beam irradiation," Tech. Phys. Lett. **45**, 281–284 (2019).

[33]J. Achard, V. Jacques, and A. Tallaire, "Chemical vapour deposition diamond single crystals with nitrogen-vacancy centres: A review of material synthesis and technology for quantum sensing applications," J. Phys. D: Appl. Phys. **53**, 313001 (2020).

[34]F. K. de Theije, J. J. Schermer, and W. J. P. van Enckevort, "Effects of nitrogen impurities on the CVD growth of diamond: Step bunching in theory and experiment," Diamond Relat. Mater. **9**, 1439–1449 (2000).

[35]A. Tallaire, M. Lesik, V. Jacques, S. Pezzagna, V. Mille, O. Brinza, J. Meijer, B. Abel, J. F. Roch, A. Gicquel, and J. Achard, "Temperature dependent creation of nitrogen-vacancy centers in single crystal CVD diamond layers," Diamond Relat. Mater. **51**, 55–60 (2015).

[36]S. A. Meynell, C. A. McLellan, L. B. Hughes, W. Wang, T. E. Mates, K. Mukherjee, and A. C. Bleszynski Jayich, "Engineering quantum-coherent defects: The role of substrate miscut in chemical vapor deposition diamond growth," Appl. Phys. Lett. **117**, 194001 (2020).

[37]J. Koike, D. M. Parkin, and T. E. Mitchell, "Displacement threshold energy for type IIa diamond," Appl. Phys. Lett. **60**, 1450–1452 (1992).

[38]B. Campbell and A. Mainwood, "Radiation damage of diamond by electron and gamma irradiation," Phys. Status Solidi A **181**, 99–107 (2000).

[39]J. F. Ziegler, M. D. Ziegler, and J. P. Biersack, "SRIM—The stopping and range of ions in matter," Nucl. Instrum. Methods Phys. Res., Sect. B **268**, 1818–1823 (2010).

[40]R. G. Wilson and S. W. Novak, "Systematics of secondary-ion-mass spectrometry relative sensitivity factors versus electron affinity and ionization potential for a variety of matrices determined from implanted standards of more than 70 elements," J. Appl. Phys. **69**, 466–474 (1991).

[41]V. Ranjan, S. Probst, B. Albanese, T. Schenkel, D. Vion, D. Esteve, J. J. L. Morton, and P. Bertet, "Electron spin resonance spectroscopy with femtoliter detection volume," Appl. Phys. Lett. **116**, 184002 (2020).

[42]C. Osterkamp, P. Balasubramanian, G. Wolff, T. Teraji, M. Nesladek, and F. Jelezko, "Benchmark for synthesized diamond sensors based on isotopically engineered nitrogen-vacancy spin ensembles for magnetometry applications," Adv. Quantum Technol. **3**, 2000074 (2020).

[43]G. Davies, "The Jahn–Teller effect and vibronic coupling at deep levels in diamond," Rep. Prog. Phys. **44**, 788–830 (1981).

[44]D. Bluvstein, Z. Zhang, C. A. McLellan, N. R. Williams, and A. C. Bleszynski Jayich, "Extending the quantum coherence of a near-surface qubit by coherently driving the paramagnetic surface environment," Phys. Rev. Lett. **123**, 146804 (2019).

[45]P. Maletinsky, S. Hong, M. S. Grinolds, B. Hausmann, M. D. Lukin, R. L. Walsworth, M. Loncar, and A. Yacoby, "A robust scanning diamond sensor for nanoscale imaging with single nitrogen-vacancy centres," Nat. Nanotechnol. **7**, 320–324 (2012).

[46]M. Pelliccione, A. Jenkins, P. Ovartchaiyapong, C. Reetz, E. Emmanouilidou, N. Ni, and A. C. Bleszynski Jayich, "Scanned probe imaging of nanoscale magnetism at cryogenic temperatures with a single-spin quantum sensor," Nat. Nanotechnol. **11**, 700–705 (2016).

[47]D. Englund, B. Shields, K. Rivoire, F. Hatami, J. Vučković, H. Park, and M. D. Lukin, "Deterministic coupling of a single nitrogen vacancy center to a photonic crystal cavity," Nano Lett. **10**, 3922–3926 (2010).